J. Fluid Mech. (1977), *vol.* 79, *part* 3, *pp.* 609–624
Printed in Great Britain

Computing internal viscous flow problems for the circle by integral methods

By R. D. MILLS

Computing Science Department, Glasgow University, Scotland

(Received 16 November 1973 and in revised form 3 September 1976)

Steady two-dimensional viscous motion within a circular cylinder generated by (*a*) the rotation of part of the cylinder wall and (*b*) fluid entering and leaving through slots in the wall is considered. Studied in particular are moving-surface problems with continuous and discontinuous surface speeds, simple inflow–outflow problems and the impinging-jet problem within a circle. The analytical solutions at zero Reynolds number are given for the last two types of problem. Numerical results are obtained at various Reynolds numbers from the integral representation of the solution. At zero Reynolds number this approach involves a quadrature around the circumference of the cylinder. At other Reynolds numbers it involves an iterative–integral technique based on the use of the 'clamped-plate' biharmonic Green's function.

1. Introduction

Streaming flows past a circular cylinder have an extensive literature, whereas flows occurring within a single circular cylinder have received comparatively little attention. No solution of the external streaming-flow problem exists at zero Reynolds number (Stokes' paradox), but this is not true of the interior problem. The solution can be given as an integral around the circumference of the cylinder or as an infinite series. It can be given in closed form in some special cases. These internal flows may occur through (*a*) the rotation of part (or all) of the cylinder wall or (*b*) fluid entering and leaving the cylinder normal to the wall. These problems are of interest physically as they are representative of two distinct types of motion which occur frequently in practice. Type (*a*) problems arise in the recirculating motion in cavities in aerodynamic surfaces (Batchelor 1956; Squire 1956), while type (*b*) problems arise, for instance, in the ventilation of confined spaces (Baturin 1959).

Rayleigh (1893) seems to have been the first to consider these fluid motions mathematically and derived analytical solutions for simplified type (*a*) and type (*b*) problems. Mabey (1957) gave the analytical solution at zero Reynolds number for a physically realistic type (*a*) problem, Burgraff (1966) later constructing a solution for arbitrary Reynolds number from an Oseen-type linearization of the full equations of motion. Further type (*a*) problems have been computed by Kuwahara & Imai (1969), while Dennis (1974) has computed a problem of type (*b*). The present paper gives analytical and numerical results for certain type (*a*) and type (*b*) problems.

In contrast to the usual finite-difference approach, it is of interest to compute these internal flows from their integral representation, both at zero Reynolds number and at Reynolds numbers in the intermediate range. The case of zero Reynolds number requires only a quadrature around the circumference of the cylinder. The case of intermediate Reynolds numbers involves the development of an *iterative–integral* technique which is based on the use of the biharmonic Green's function. This technique will be described in this paper. Harmonic Green's functions have been used in viscous flow computation (Panniker & Lavan 1975), but this approach still requires the use of the finite-difference method for the solution of the vorticity equation.

2. Governing equations

With a suitable length and speed to define non-dimensional variables the equation of steady viscous incompressible fluid flow is

$$(\mathbf{q}.\nabla)\,\mathbf{q} = -\nabla p + R^{-1}\nabla^2\mathbf{q}, \tag{1}$$

where $\mathbf{q}$ is the velocity vector, p is the pressure and R is the Reynolds number of the motion.

Consider two-dimensional motion and take plane polar co-ordinates (r, θ) with velocity components (u_r, u_θ) such that the vorticity vector $\boldsymbol{\zeta} = \operatorname{curl}\mathbf{q}$ has only one component

$$\zeta = \frac{1}{r}\frac{\partial(ru_\theta)}{\partial r} - \frac{1}{r}\frac{\partial u_r}{\partial\theta}, \tag{2}$$

normal to the r, θ plane. If a stream function ψ is introduced by

$$u_r = r^{-1}\,\partial\psi/\partial\theta, \quad u_\theta = -\partial\psi/\partial r, \tag{3}$$

then the equation of continuity

$$\frac{1}{r}\frac{\partial(ru_r)}{\partial r} + \frac{1}{r}\frac{\partial u_\theta}{\partial\theta} = 0 \tag{4}$$

is satisfied automatically. On introducing (3) into (2) and taking the curl of both sides of (1), we find that the equations of motion take the form

$$\nabla^2\psi = -\zeta, \tag{5}$$

$$\nabla^2\zeta = R\left[\frac{1}{r}\frac{\partial\psi}{\partial\theta}\frac{\partial\zeta}{\partial r} - \frac{1}{r}\frac{\partial\psi}{\partial r}\frac{\partial\zeta}{\partial\theta}\right], \tag{6}$$

where

$$\nabla^2 \equiv \frac{\partial^2}{\partial r^2} + \frac{1}{r}\frac{\partial}{\partial r} + \frac{1}{r^2}\frac{\partial^2}{\partial\theta^2}.$$

This coupled pair of second-order elliptic equations (5) and (6) for ψ and ζ may be combined into the single fourth-order nonlinear equation

$$\nabla^4\psi = -Rr^{-1}\,\partial(\psi, \nabla^2\psi)/\partial(r, \theta) = -R\,J(\psi, \nabla^2\psi), \tag{7}$$

where $\nabla^4 \equiv \nabla^2(\nabla^2)$ is the biharmonic operator and J is the Jacobian operator. For slow viscous flow ($R \to 0$), (7) reduces to the biharmonic equation

$$\nabla^4\psi = 0. \tag{8}$$

3. Slow viscous flow solutions

Now consider the motion inside a circular cylinder of radius a whose centre is at the origin of the co-ordinates. Series solutions can be constructed from the following fundamental solutions of the biharmonic equation attributed to Michell (1899) (e.g. see Timoshenko & Goodier 1951, p. 116):

$$\psi = a_0 + b_0 r^2 + \sum_{n=1}^{\infty} (a_n r^n + b_n r^{n+2}) \cos n\theta + \sum_{n=1}^{\infty} (c_n r^n + d_n r^{n+2}) \sin n\theta. \quad (9)$$

The coefficients a_i, b_i, c_i and d_i have to be determined by satisfying the boundary conditions of the present problems, viz.

$$\psi = f(\theta), \qquad \partial\psi/\partial r = -u_\theta = g(\theta) \quad \text{on} \quad r = 1. \quad (10), (11)$$

By the method that is used to derive Poisson's integral formula from its Fourier-series form (e.g. see Dennemeyer 1968, p. 107), it can readily be established that the above series solution is equivalent to the integral solution

$$\psi(r,\theta) = \frac{(1-r^2)^2}{2\pi} \int_0^{2\pi} \left[\frac{[1 - r\cos(\phi-\theta)] f(\phi)}{[1 - 2r\cos(\phi-\theta) + r^2]^2} - \frac{\frac{1}{2} g(\phi)}{1 - 2r\cos(\phi-\theta) + r^2} \right] d\phi. \quad (12)$$

This solution is of course well known in the theory of elasticity. It is worth observing that (12) can also be built up with the aid of Poisson's integral by looking for a solution of the form

$$\psi = (r^2 - 1)\psi_1 + \psi_2, \quad (13)$$

where ψ_1 and ψ_2 are harmonic functions (e.g. see Tychonov & Samarski 1964, p. 361).

Moving-wall problems

In these problems the motion is completely enclosed and is generated by the rotation of part of the circumference. Here we use the radius of the cylinder and the (constant) speed on the moving part of the surface to define non-dimensional variables, so that the Reynolds number of the motion is

$$R_M = Ua/\nu \quad (14)$$

(see figure 1). Rayleigh (1893) appears to have been the first to give a solution at $R_M = 0$ for a problem of this kind. His solution corresponds to the application of an infinite tangential speed over an infinitely small arc. The solution for the more practical case of a finite length of arc moving at finite speed seems to have been first given by Mabey (1957). At high Reynolds numbers this type of flow, i.e. cavity flow', has been suggested as a model for the motion in real physical cavities (Batchelor 1956; Squire 1956). The present author has given theoretical and experimental results and also solved the equations of motion numerically for some special cases of this type of flow (e.g. see Mills 1964, 1965).

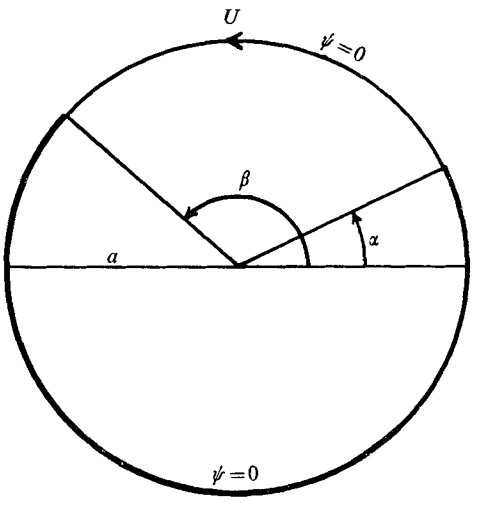

FIGURE 1. Moving-surface problem.

The boundary conditions (10) and (11) are here

$$f = 0, \quad 0 \leqslant \theta \leqslant 2\pi, \tag{15}$$

$$g = \begin{cases} -1, & \alpha < \theta < \beta, \\ 0, & \beta < \theta < 2\pi+\alpha. \end{cases} \tag{16}$$

The solution is readily found from (9) to be

$$\psi = \frac{(1-r^2)}{4\pi}\left[\beta-\alpha+2\sum_{n=1}^{\infty}\left(\frac{\sin n\beta-\sin n\alpha}{n}\right)r^n\cos n\theta + 2\sum_{n=1}^{\infty}\left(\frac{\cos n\alpha-\cos n\beta}{n}\right)r^n\sin n\theta\right]. \tag{17}$$

From (12) it is easy to derive the closed-form version of this solution:

$$\psi = \frac{(1-r^2)}{2\pi}\left[\gamma+\tan^{-1}\left(\frac{1+r}{1-r}\tan\frac{\beta-\theta}{2}\right)-\tan^{-1}\left(\frac{1+r}{1-r}\tan\frac{\alpha-\theta}{2}\right)\right], \tag{18}$$

where

$$\gamma = \begin{cases} 0, & \beta-\pi < \theta < \alpha+\pi, \\ \pi, & \alpha+\pi < \theta < \beta+\pi, \end{cases}$$

and the Cauchy principal value of the integral has been used. These solutions were first given, in a slightly different form, by Mabey (1957).

In the case $\alpha = 0$, $\beta = \pi$, the streamlines of the motion have been computed from the integral representation (12) using the boundary conditions (15) and (16). The trapezium rule was used for the quadrature. As the boundary conditions involve discontinuous changes, it was not considered worth while to use a more accurate quadrature formula. The interval of integration was simply reduced progressively until a prescribed accuracy was obtained in the solution at every computed point in the flow field. The results were checked against the series representation (17) and also against the closed form (18). Roughly similar com-

puting times were required to determine the solution to a given accuracy from the integral representation and the infinite-series representation, these representations sharing the property that it takes longer to compute the solution at points near the boundary than at points near the centre of the circle. The streamlines are given in figure 4(*a*). A similar figure was produced by Mabey with the aid of a geometrical representation of the solution (18). Mabey also photographed the motion in an experiment and his experimental streamlines are in good agreement with the theoretical streamlines.

A very simple example of this kind of flow has been given by Kuwahara & Imai (1969). It corresponds to the zero Reynolds number solution

$$\psi = \tfrac{1}{4}(1-r^2)(1+r\cos\theta), \tag{19}$$

with the boundary velocity function

$$g(\theta) = -\tfrac{1}{2}(1+\cos\theta). \tag{20}$$

This flow would be difficult to realize in practice, but it affords a simple test for our numerical methods. Moreover, it is a very convenient test for the numerical verification of Batchelor's (1956) constant-vorticity theorem. For this problem, the constant vorticity of the core at large Reynolds numbers can easily be shown to be

$$\zeta_0 = (\tfrac{3}{2})^{\frac{1}{2}}, \tag{21}$$

following Wood (1957).

Inflow–outflow problems

We now consider problems where $\partial\psi/\partial r = 0$ and ψ is specified along the boundary, in particular the class of problems defined in figure 2. First, consider the simple inflow–outflow problem corresponding to $\epsilon'' = \epsilon''' = 0$. Use the radius a, the speed U and half the flow $Ua\epsilon$ across the arc DC (or AB) to define non-dimensional variables. The Reynolds number of the flow is then

$$R_I = Ua\epsilon/\nu, \tag{22}$$

where ν is the kinematic viscosity coefficient of the fluid.

For this problem, the boundary conditions (10) and (11) are

$$f = \begin{cases} 1+\epsilon'^{-1}(\theta-\alpha), & \alpha-\epsilon' < \theta < \alpha+\epsilon', \\ 2, & \alpha+\epsilon' < \theta < \beta-\epsilon, \\ 1+\epsilon^{-1}(\beta-\theta), & \beta-\epsilon < \theta < \beta+\epsilon, \\ 0, & \beta+\epsilon < \theta < 2\pi+\alpha, \end{cases} \tag{23}$$

and

$$g(\theta) = 0, \quad 0 \leqslant \theta \leqslant 2\pi. \tag{24}$$

The Fourier coefficients in (9) then become

$$\left.\begin{aligned} a_0 &= \pi^{-1}(\beta-\alpha), \quad b_0 = 0, \\ a_n &= -\frac{n+2}{\pi n^2}\left(\frac{\sin n\epsilon'}{\epsilon'}\sin n\alpha - \frac{\sin n\epsilon}{\epsilon}\sin n\beta\right), \quad b_n = -\frac{n}{n+2}a_n, \\ c_n &= -\frac{n+2}{\pi n^2}\left(\frac{\sin n\epsilon'}{\epsilon'}\cos n\alpha - \frac{\sin n\epsilon}{\epsilon}\cos n\beta\right), \quad d_n = -\frac{n}{n+2}c_n. \end{aligned}\right\} \tag{25}$$

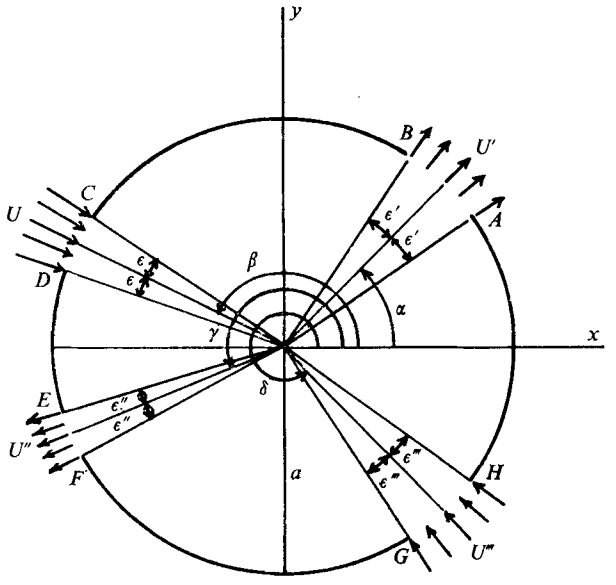

FIGURE 2. Inflow–outflow problem.

The streamlines of the motion for the two cases $\alpha = 0, \beta = \pi, \epsilon = \epsilon' = \frac{1}{32}\pi$ and $\alpha = \frac{1}{8}\pi, \beta = \pi, \epsilon = \epsilon' = \frac{1}{32}\pi$ were first computed from the integral representation of the solution (12) with $f(\theta)$ and $g(\theta)$ given by (23) and (24), using the trapezium rule as before. These results were then checked by computing the solution from the infinite series. Only the results for the second case are given here (see figure 6*a*), as the first (symmetric) case has now been given by Dennis (1974). In passing, we remark that Rayleigh's solution corresponds to our inlet and outlet shrinking in size until they become a point source and sink respectively, at opposite ends of the horizontal diameter in the case $\alpha = 0, \beta = \pi$.

Next, consider the problem which corresponds to setting $\epsilon' = \epsilon'' = \epsilon''' = \epsilon$, $U' = U'' = U''' = U$, $\alpha = \frac{1}{2}\pi$, $\beta = \pi$, $\gamma = \frac{3}{2}\pi$ and $\delta = 2\pi$. This case is of fundamental interest in that it involves the direct impact of two viscous jets. With the same non-dimensional variables as before, the boundary conditions are

$$f = \begin{cases} 1-\theta/\epsilon, & -\epsilon < \theta < \epsilon, \\ 0, & \epsilon < \theta < \frac{1}{2}\pi - \epsilon, \\ 1+\epsilon^{-1}(\theta - \frac{1}{2}\pi), & \frac{1}{2}\pi - \epsilon < \theta < \frac{1}{2}\pi + \epsilon, \\ 2, & \frac{1}{2}\pi + \epsilon < \theta < \pi - \epsilon, \\ 1+\epsilon^{-1}(\pi - \theta), & \pi - \epsilon < \theta < \pi + \epsilon, \\ 0, & \pi + \epsilon < \theta < \frac{3}{2}\pi - \epsilon, \\ 1+\epsilon^{-1}(\theta - \frac{3}{2}\pi), & \frac{3}{2}\pi - \epsilon < \theta < \frac{3}{2}\pi + \epsilon, \\ 2, & \frac{3}{2}\pi + \epsilon < \theta < 2\pi - \epsilon, \end{cases} \tag{26}$$

and

$$g(\theta) = 0, \quad 0 \leqslant \theta \leqslant 2\pi. \tag{27}$$

The Fourier coefficients for this problem are then

$$\left.\begin{aligned} &a_0 = 1, \quad b_0 = 0, \quad a_n = 0, \quad b_n = 0, \\ &c_n = \frac{n+2}{\pi n^2}\frac{\sin n\epsilon}{\epsilon}\left(-1+\cos\frac{n\pi}{2}-\cos n\pi+\cos\frac{3n\pi}{2}\right), \quad d_n = -\frac{n}{n+2}c_n. \end{aligned}\right\} \tag{28}$$

The streamlines were computed from (9) and (28) and also from the integral representation and the results are given in figure 7 (*a*). The streamlines are shown only in the first quadrant, because of symmetry.

The attractive feature of the boundary-integral method for computing the present slow viscous flow problems is the comparative ease with which it can handle complicated boundary-condition functions $f(\theta)$ and $g(\theta)$, since only a quadrature around the circumference is required. Care should of course be exercised in the choice of quadrature formula depending on the nature of $f(\theta)$ and $g(\theta)$. For instance, one should use the trapezium rule with small intervals if these functions have any step discontinuities, as in the present examples. It should be noted that adequate handling of the boundary conditions of inflow–outflow problems with narrow inlets or outlets by other numerical methods presents rather greater difficulties, such as the need for intensive local mesh refinement in the finite-difference approach.

4. Numerical solutions at non-zero Reynolds numbers

Green's function method

The basic idea is to construct a solution in integral form with the aid of the appropriate Green's function. Starting from Green's identity, we can easily derive the relation (see Garabedian 1964, chap. 7)

$$\iint_D [\psi\nabla^4\chi - \chi\nabla^4\psi]\,dx\,dy = \int_C \left[\psi\frac{\partial\nabla^2\chi}{\partial n} - \nabla^2\chi\frac{\partial\psi}{\partial n} + \nabla^2\psi\frac{\partial\chi}{\partial n} - \chi\frac{\partial\nabla^2\psi}{\partial n}\right]ds, \tag{29}$$

where D is some closed region of the x, y plane with boundary curve C whose outward normal is denoted by n, as in figure 3. Now associate χ with the *biharmonic Green's function* G defined by

$$\left.\begin{aligned} \nabla^4 G &= \delta(x-\xi, y-\eta) \quad \text{in} \quad D, \\ G &= \partial G/\partial n = 0 \quad\quad \text{on} \quad C, \end{aligned}\right\} \tag{30}$$

where δ is the Dirac delta function. Then from (29) the solution of the inhomogeneous boundary-value problem

$$\left.\begin{aligned} \nabla^4\psi &= F(x,y) \quad\quad\quad \text{in} \quad D, \\ \psi = f(s), \quad \partial\psi/\partial n &= g(s) \quad \text{on} \quad C \end{aligned}\right\} \tag{31}$$

can be put into the form

$$\psi(x,y) = \iint_D G(x,y;\xi,\eta)\,F(\xi,\eta)\,d\xi\,d\eta + \psi^0(x,y), \tag{32}$$

where

$$\psi^0(x,y) = \int_C \left[f(s)\frac{\partial\nabla^2 G}{\partial n} - \nabla^2 G\,g(s)\right]ds \tag{33}$$

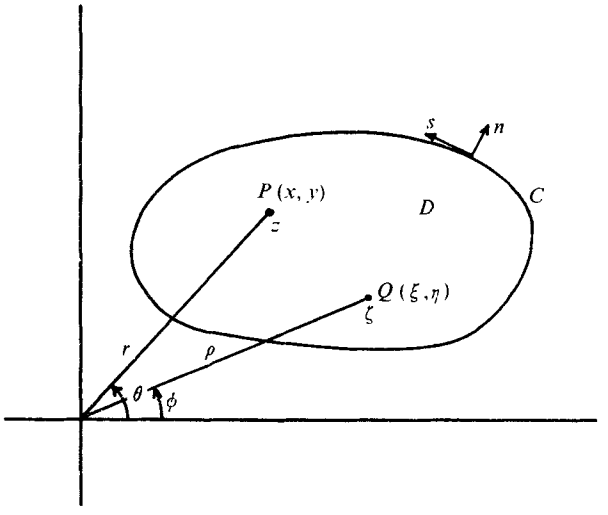

FIGURE 3. General closed region.

is the solution of the *first biharmonic boundary-value problem*

$$\left.\begin{aligned} \nabla^4\psi^0 &= 0 \qquad \text{in } D, \\ \psi^0 = f(s), \quad \partial\psi^0/\partial n &= g(s) \quad \text{on } C. \end{aligned}\right\} \tag{34}$$

The solution of the *linear* boundary-value problem (31) thus reduces to the determination of the biharmonic Green's function G for the appropriate region D. This approach is of course well known in the theory of elasticity.

To apply this method to the *nonlinear* Navier–Stokes equation (7), we can regard the right-hand side of (7) as a known function at each cycle k of the iterative process:

$$\psi^{k+1}(x,y) = -R\iint_D G(x,y;\xi,\eta)\,J(\psi^k(\xi,\eta),\nabla^2\psi^k(\xi,\eta))\,d\xi\,d\eta + \psi^0(x,y). \tag{35}$$

Equation (35) is thus made the basis of a numerical method for solving the Navier–Stokes equations. This simple notion of an *iterative–integral* (i.e. Picard-type) method has also been used successfully by the present author for solving the laminar boundary-layer equations (Mills 1974).

The main analytical difficulty in the present approach is of course the determination of the biharmonic Green's function for a general region D. However, this function can easily be obtained for a circular region. In terms of the complex variables $z = x+iy$ and $\zeta = \xi+i\eta$ the result is (see Garabedian 1964, p. 272)

$$G(z,\zeta) = \frac{1}{8\pi}|z-\zeta|^2 \ln\left|\frac{z-\zeta}{1-\bar{\zeta}z}\right| + \frac{1}{16\pi}(|z|^2-1)(|\zeta|^2-1), \tag{36}$$

where the overbar denotes the complex conjugate and ζ is not to be confused with the vorticity. If we change to polar co-ordinates given by $z = re^{i\theta}$ and $\zeta = \rho e^{i\phi}$, we find after some routine manipulation that (35) takes the form

$$\psi^{k+1}(r,\theta) = -R\int_0^{2\pi}\int_0^1 G(r,\theta;\rho,\phi)\,J(\psi^k(\rho,\phi),\nabla^2\psi^k(\rho,\phi))\,\rho\,d\rho\,d\phi + \psi^0(r,\theta), \tag{37}$$

where

$$G = \frac{1}{16\pi}[\rho^2 + r^2 - 2\rho r\cos(\phi-\theta)]\ln\left[\frac{\rho^2+r^2-2\rho r\cos(\phi-\theta)}{1+\rho^2 r^2-2\rho r\cos(\phi-\theta)}\right] + \frac{1}{16\pi}(r^2-1)(\rho^2-1) \tag{38}$$

and ψ^0 is given by (12).

The numerical method of solution is as follows. The slow viscous flow solution ψ^0 is used as the 'starting' ($k = 0$) solution in the above iterative scheme. A separate field is used for the vorticity $\zeta = -\nabla^2\psi$. For all mesh points except those on the circle C^- one radial mesh length δr from the boundary, the Jacobian is computed using the usual central-difference formulae for the derivatives. We use ψ_{ij} to denote $\psi(i\delta r, j\delta\theta)$, etc., and let m and n be the number of intervals in the circumferential and radial directions respectively. For points on C^- the $\partial\zeta/\partial\rho$ term in the Jacobian is replaced using the three-point 'backward-difference' formula (accurate to order $(\delta\rho)^2$)

$$\left(\frac{\partial\zeta}{\partial\rho}\right)_{n-1,j} = \frac{1}{2\delta\rho}(3\zeta_{n-1,j} - 4\zeta_{n-2,j} + \zeta_{n-3,j}) \tag{39}$$

to avoid the necessity of knowing the boundary values of ζ, as is required in the finite-difference methods. (Such a requirement would defeat the purpose of using the integral representation (37) and (38), which has the appropriate boundary conditions already 'built in'.) The double integral in (37) is computed with the aid of the very simple quadrature formula

$$\int_0^{2\pi}\int_0^1 f(\rho,\phi)\,\rho\,d\rho\,d\phi = \delta\rho\,\delta\phi\sum_{i=1}^{n-1}\sum_{j=1}^{m}\rho_i f_{ij} \tag{40}$$

derived by applying the trapezium rule to the variables ρ and ϕ in turn and observing that the integrand $f \equiv GJ$ vanishes on the boundary circle, where $i = n$. Our method requires a *source point* $Q(i'\delta\rho, j'\delta\phi)$ to coincide with an *argument point* $P(i\delta r, j\delta\theta)$ once for each double integration with respect to ρ and ϕ. Even though the biharmonic Green's function G vanishes it is still *singular* when $P = Q$ (giving the fundamental biharmonic singularity, in fact), and consequently it was not considered worth while to use a more accurate quadrature formula.

To obtain convergence we had to use two relaxation factors ω and ω' for the ζ and ψ fields:

$$\zeta_{ij}^{k+1} = \omega\zeta_{ij}^{*k+1} + (1-\omega)\zeta_{ij}^{k}, \tag{41}$$

$$\psi_{ij}^{k+1} = \omega'\psi_{ij}^{*k+1} + (1-\omega')\psi_{ij}^{k}, \tag{42}$$

where the starred quantities represent the 'theoretical' values at each cycle. We were guided in this by the need to use two relaxation factors in the iterative–integral method of solution of the boundary-layer equations (Mills 1974). The iteration was continued until a suitable convergence criterion was satisfied (e.g. as in Mills 1968). The final solution was always checked *independently* by applying the standard finite-difference formula

$$\zeta_{ij} = \frac{1}{2}\left\{1 + \frac{1}{(i\delta\theta)^2}\right\}^{-1}\left[\left(1+\frac{1}{2i}\right)\zeta_{i+1,j} + \frac{1}{(i\delta\theta)^2}\zeta_{i,j+1} + \left(1-\frac{1}{2i}\right)\zeta_{i-1,j} + \frac{1}{(i\delta\theta)^2}\zeta_{i,j-1}\right.$$
$$\left. - \frac{R}{4}\frac{1}{i\delta\theta}\{(\psi_{i,j+1}-\psi_{i,j-1})(\zeta_{i+1,j}-\zeta_{i-1,j}) - (\psi_{i+1,j}-\psi_{i-1,j})(\zeta_{i,j+1}-\zeta_{i,j-1})\}\right] \tag{43}$$

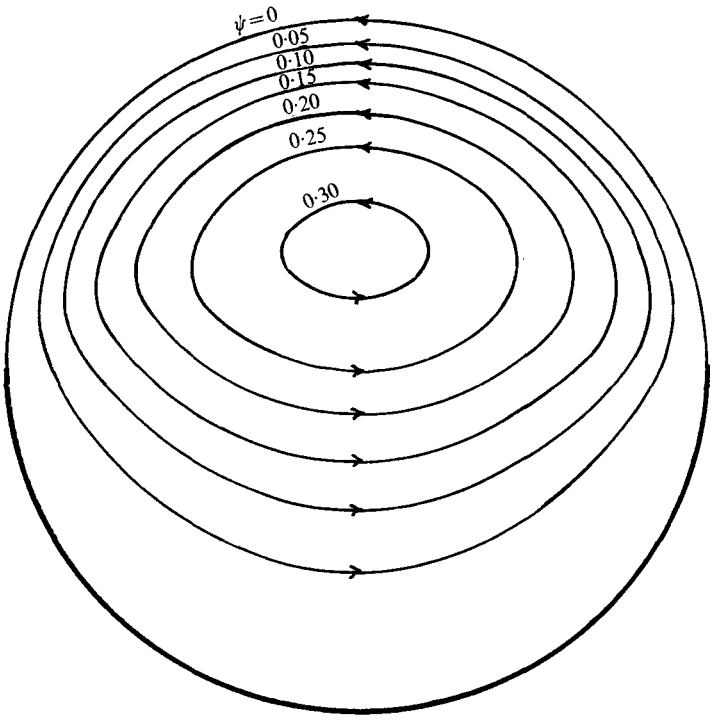

(a)

FIGURE 4. Moving-surface problems. (a) $g(\theta)$ given by (16); $R_M = 0$. (b) $g(\theta)$ given by (16); $R_M = 25$, $\delta r = \frac{1}{10}$, $\delta\theta = \frac{1}{20}\pi$, $\omega = 0{\cdot}3$, $\omega' = 0{\cdot}3$. (c) $g(\theta) = -\frac{1}{2}(1+\cos\theta)$; $R_M = 16$, $\delta r = \frac{1}{10}$, $\delta\theta = \frac{1}{20}\pi$, $\omega = 0{\cdot}3$, $\omega' = 0{\cdot}3$. ○, Kuwahara & Imai's results.

to each nodal point at the end of the computation and comparing the results with $-\nabla^2\psi_{ij}$.

With regard to efficient programming, the Green's function $G(r_i, \theta_j; \rho_{i'}, \phi_{j'})$ can be computed once and for all and stored in a symmetric three-dimensional array, since $G(r_i, \theta_j; \rho_{i'}, \phi_{j'}) \equiv G(r_i, \rho_{i'}, |j-j'|\,\delta\theta) = G(\rho_{i'}, r_i, j''\delta\theta)$, where $\delta\theta$ is the angular mesh size. To store $G(r_i, \theta_j; \rho_{i'}, \phi_{j'})$ for all the possible permutations of (i, j, i', j') would make large demands on storage even for moderate mesh sizes. Otherwise, we should have to compute $G(r_i, \theta_j; \rho_{i'}, \phi_{j'})$ about m^2n^2 times every iteration, which would lead to large computing times because of the cosine and logarithm functions in G.

This numerical method was applied to the moving-surface problem and to the inflow–outflow problem, the cases computed being shown in figure 4 and figures 6 and 7. The appropriate mesh sizes, Reynolds numbers and relaxation factors are given in the figure captions. In the inflow–outflow problem the mesh sizes were chosen such that no mesh points coincided with the sharp edges, while in the moving-surface problem with discontinuities (figure 4*b*) the co-ordinate system was rotated relative to the boundary by half the angular mesh size to avoid the discontinuities.

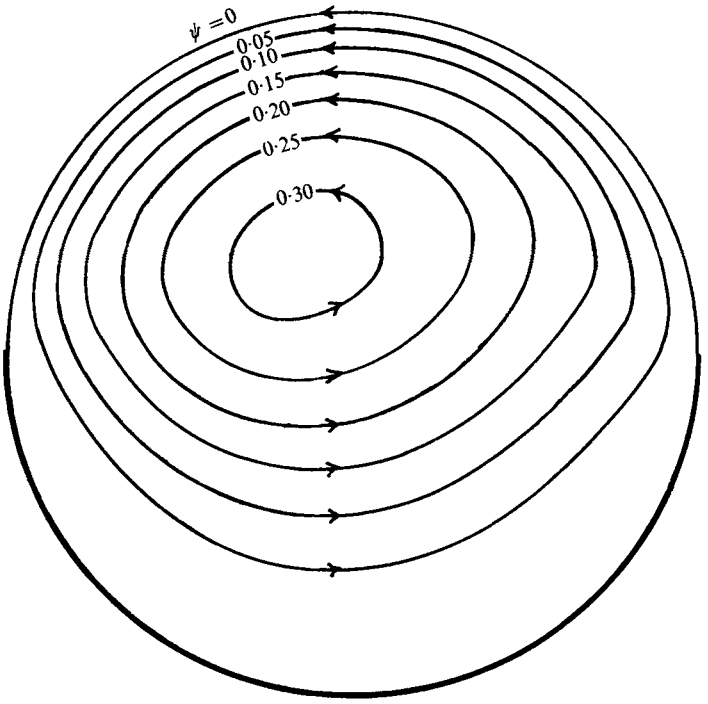

(*b*)

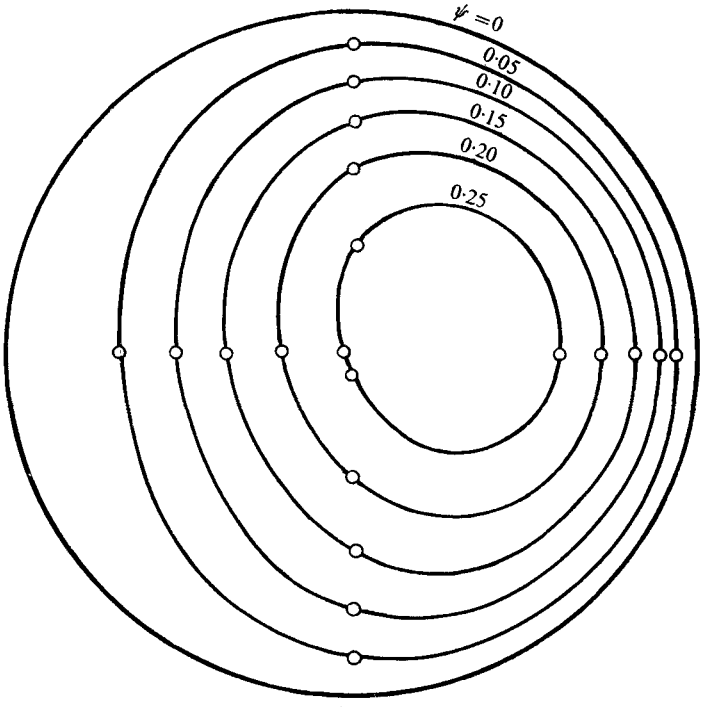

(*c*)

FIGURES 4(*b*), (*c*). For legend see p. 618.

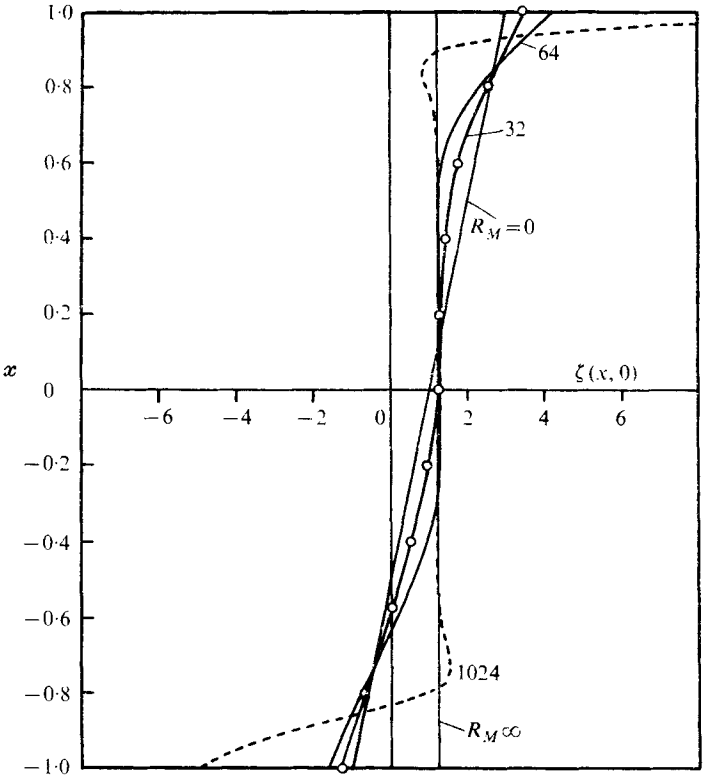

FIGURE 5. Vorticity distribution on x axis. ○, ---, Kuwahara & Imai's results. $g(\theta) = -\frac{1}{2}(1+\cos\theta)$.

5. Discussion of results

For the test problem of Kuwahara & Imai, our method gives results in excellent agreement with theirs (see figure 4*c*). Also presented are results for the vorticity distribution along the x axis for various Reynolds numbers (figure 5). It is clear that the vorticity in the central 'core' region is tending to the constant value given by (21). We have not attempted to carry our computation above $R_M = 64$ since our mesh Reynolds number R_δ is becoming rather high for convergence of the iterative process and small enough truncation errors. Kuwahara & Imai, however, give results for $R_M = 1024$ which certainly bear out the model with a constant-vorticity core. The moving-surface problem of Mabey was computed for $R_M = 25$ and the results are shown in figure 4(*b*). This problem is more complex in having two discontinuous changes in tangential velocity on the surface of the cylinder.

Recirculation does not occur at zero Reynolds number in the simple inflow–outflow problems computed. This is also true of Rayleigh's solution, as can easily be proved. Rayleigh made in 1893 the comment that the formation of an eddy or backwater would result from the nonlinear terms in the equation of motion. In the asymmetric case presented here it was found that the lower eddy first appears at a value of R_I somewhere between 2·4 and 2·5 (see figure 6*b*). The upper eddy

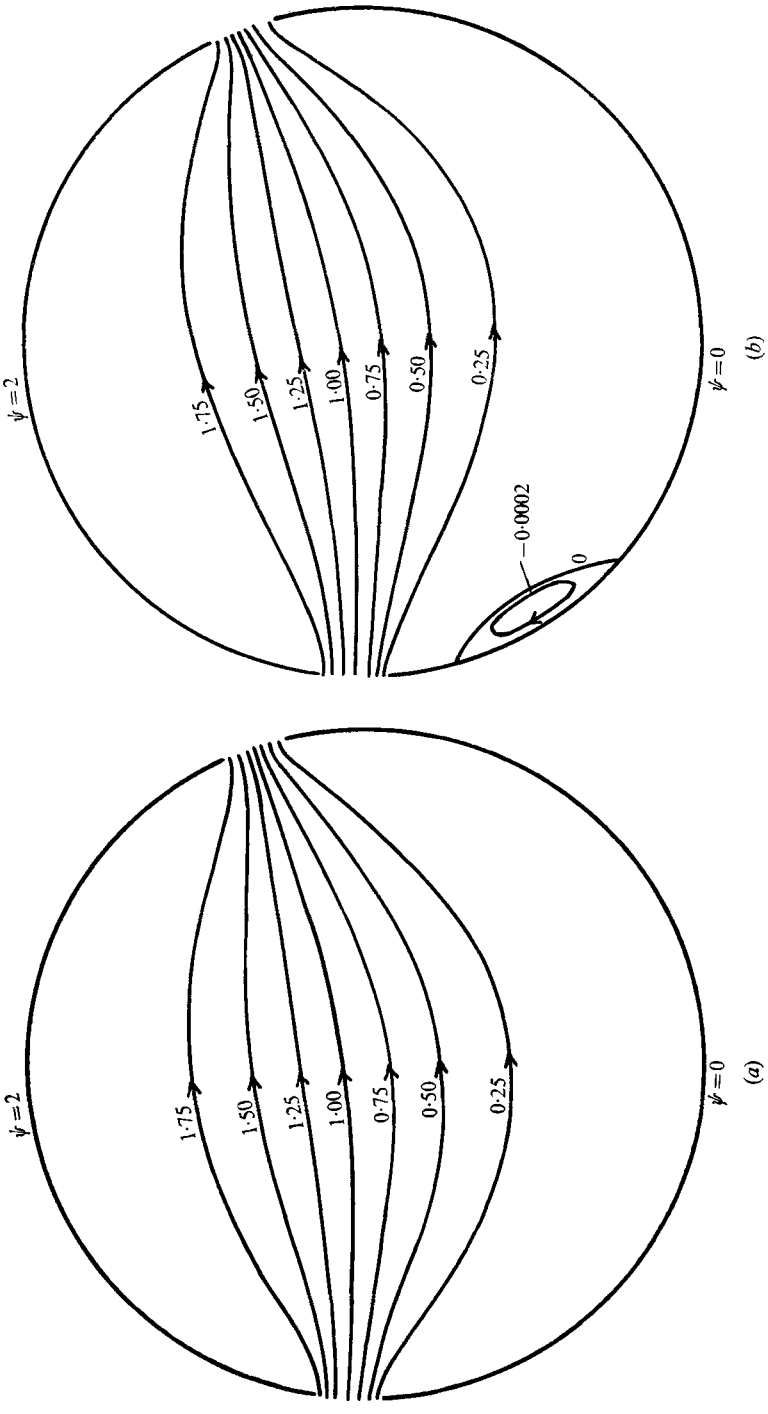

FIGURES 6 (*a*, *b*). For legend see p. 622.

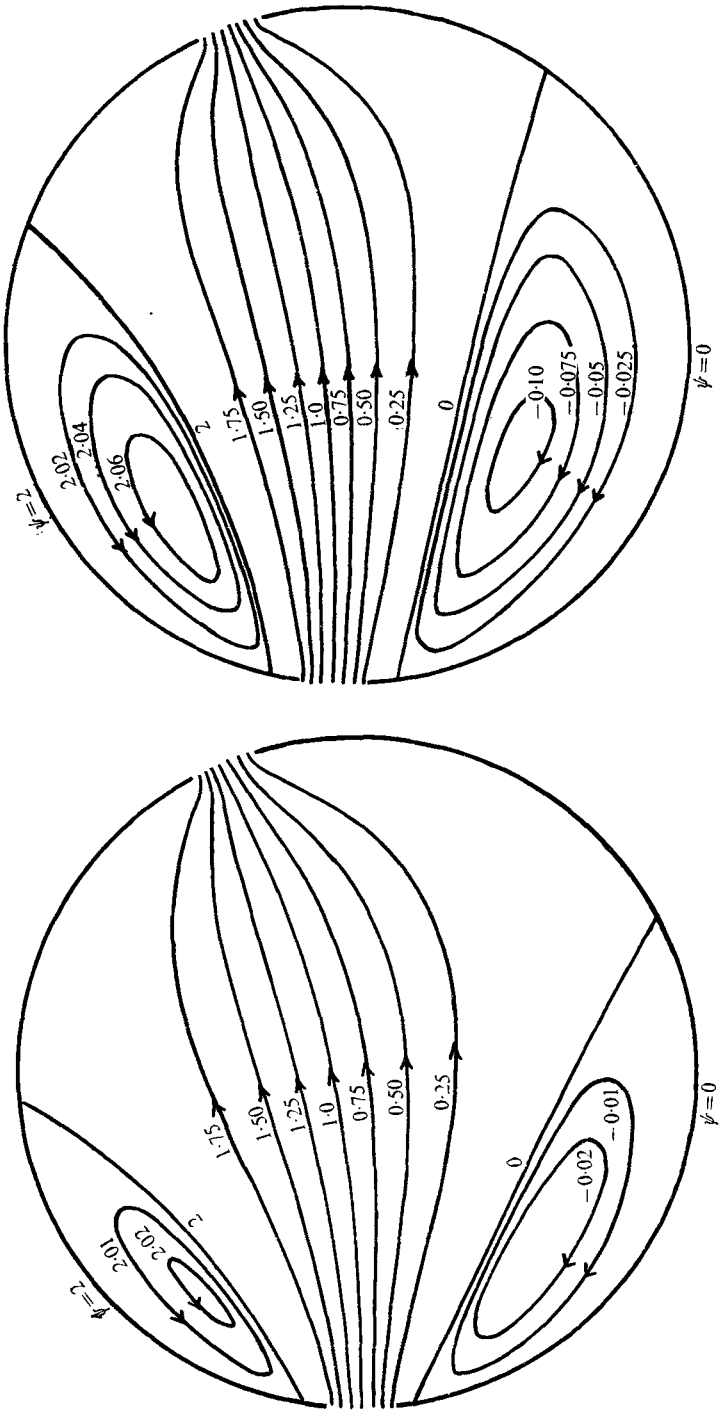

FIGURE 6. Simple inflow–outflow problem. $\alpha = \frac{1}{8}\pi, \beta = \pi, \epsilon = \epsilon' = \frac{1}{32}\pi$. (*a*) $R_I = 0$. (*b*) $R_I = 2{\cdot}5$. (*c*) $R_I = 5$. (*d*) $R_I = 7{\cdot}5$. $\delta r = \frac{1}{16}$, $\delta\theta = \frac{1}{20}\pi$, $\omega = 0{\cdot}5$, $\omega' = 0{\cdot}5$.

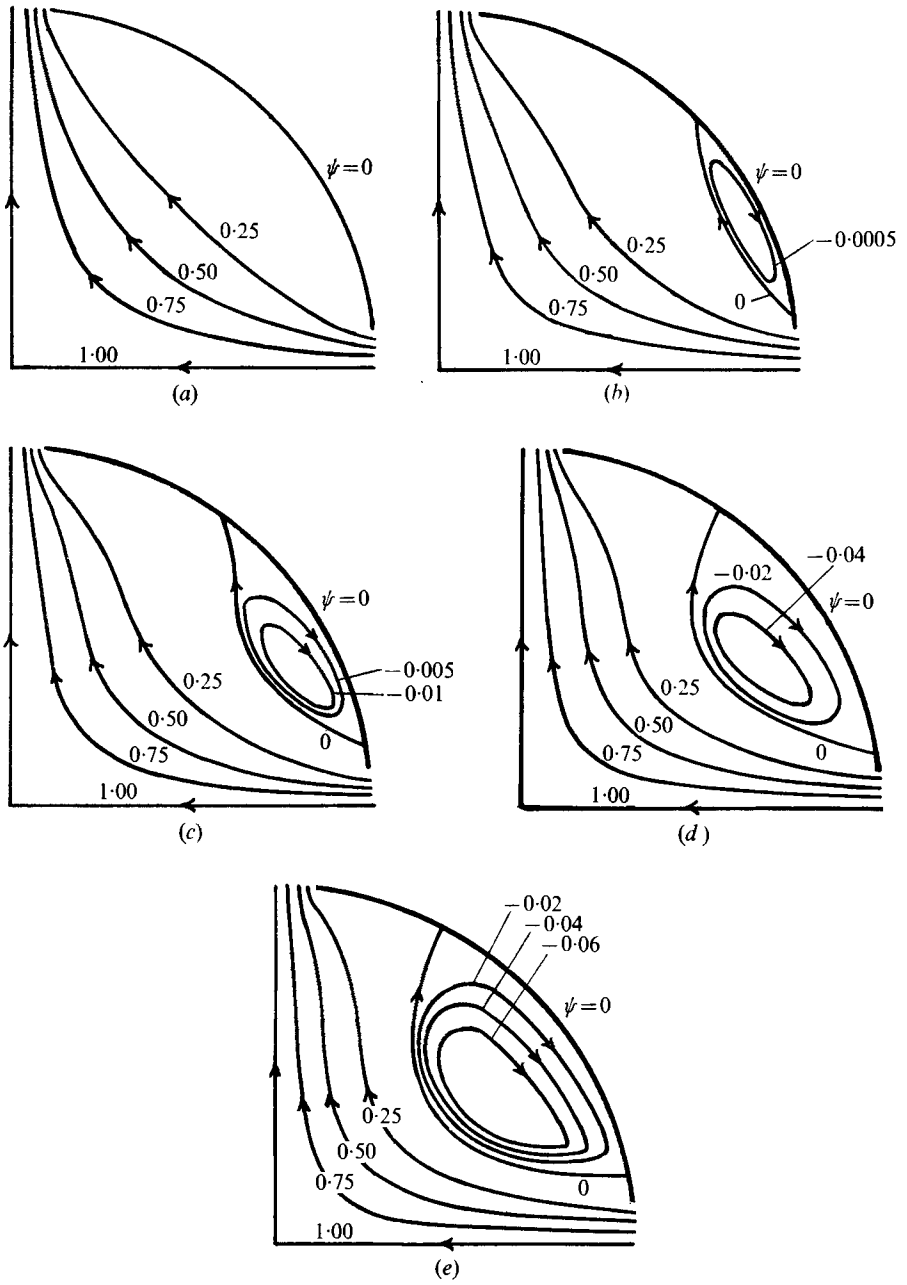

FIGURE 7. Impinging-jet problem within a circle. $\epsilon' = \epsilon'' = \epsilon''' = \epsilon = \frac{1}{32}\pi$, $U' = U'' = U''' = U$, $\alpha = \frac{1}{2}\pi$, $\beta = \pi$, $\gamma = \frac{3}{2}\pi$, $\delta = 2\pi$. (*a*) $R_I = 0$. (*b*) $R_I = 3{\cdot}5$. (*c*) $R_I = 5$. (*d*) $R_I = 7{\cdot}5$. (*e*) $R_I = 10$. $\delta r = \frac{1}{10}$, $\delta\theta = \frac{1}{20}\pi$, $\omega = 0{\cdot}5$, $\omega' = 0{\cdot}5$.

first appears at an R_I between 2·5 and 2·6, and figures 6(*c*) and (*d*) show the development of the recirculation regions as the Reynolds number increases further.

In the impinging-jet problem symmetry was preserved at all the Reynolds numbers considered (figure 7). No recirculation occurs at zero Reynolds number (figure 7*a*). The eddies first appear at a value of R_I somewhere in the interval 3·0–3·1. It is of interest that stable numerical solutions persist for Reynolds numbers up to 10 at least. However, numerical instability begins to set in at about $R_I = 15$, and this may be associated with the onset of unsteadiness in the physical flow.

In addition to the built-in check on the method, mentioned earlier, we have checked the method against results obtained by the standard finite-difference method and found good agreement. If efficiently programmed, the method is comparable to the standard method in overall computational efficiency. It is especially recommended for those problems which have discontinuities and for which the analytical solutions at zero Reynolds number are known, as in the examples presented. In closing we remark that the method could be applied to regions other than the circle with the aid of the appropriate conformal transformation.

The author is grateful for the receipt of the necessary time on the Glasgow University KDF9, the NEL Univac 1108 and the Numac IBM 370/168 computers.

REFERENCES

BATCHELOR, G. K. 1956 *J. Fluid Mech.* **1**, 177.

BATURIN, W. W. 1959 *Lüftungsanlagen für Industriebauten.* Berlin: Veb Verlag Technik.

BURGRAFF, O. R. 1966 *J. Fluid Mech.* **24**, 113.

DENNEMEYER, R. 1968 *Introduction to Partial Differential Equations and Boundary Value Problems.* McGraw-Hill.

DENNIS, S. C. R. 1974 In *Proc. 4th Int. Conf. on Numerical Methods in Fluid Dyn.*, p. 138, Springer.

GARABEDIAN, P. R. 1964 *Partial Differential Equations.* Wiley.

KUWAHARA, K. & IMAI, I. 1969 *Phys. Fluids Suppl.* **12**, II-94.

MABEY, D. G. 1957 *J. Roy. Aero. Soc.* **61**, 181.

MICHELL, J. H. 1899 *Proc. Lond. Math. Soc.* **31**, 100.

MILLS, R. D. 1964 *Aero. Res. Counc. R. & M.* no. 3428.

MILLS, R. D. 1965 *J. Roy. Aero. Soc.* **69**, 714.

MILLS, R. D. 1968 *J. Mech. Engng Sci.* **10**, 133.

MILLS, R. D. 1974 *Aero. Res. Counc. R. & M.* no. 3742.

PANIKKER, P. K. G. & LAVAN, Z. 1975 *J. Comp. Phys.* **18** (1), 46.

RAYLEIGH, LORD 1893 *Phil. Mag.* **5**, 354.

SQUIRE, H. B. 1956 *J. Roy. Aero. Soc.* **60**, 203.

TIMOSHENKO, S. & GOODIER, J. N. 1951 *Theory of Elasticity*, 2nd edn. McGraw-Hill.

TYCHONOV, A. N. & SAMARSKI, A. A. 1964 *Partial Differential Equations of Mathematical Physics*, vol. 1 (trans.). San Francisco: Holden-Day.

WOOD, W. W. 1957 *J. Fluid Mech.* **2**, 77.